Breakup of rotating asymmetric quartic-quadratic trapped condensates

Leonardo Brito,[1,*] Alex Andriati,[1,†] Lauro Tomio,[2,‡] and Arnaldo Gammal[1,§]
[1]*Instituto de Física, Universidade de São Paulo, 05508-090 São Paulo, Brazil*
[2]*Instituto de Física Teórica, Universidade Estadual Paulista, 01156-970 São Paulo, SP, Brazil*

(Received 17 November 2020; accepted 15 December 2020; published 29 December 2020)

The threshold conditions for a rotating pancakelike asymmetric quartic-quadratic confined condensate to break in two localized fragments, as well as to produce a giant vortex at the center within the vortex-pattern distributions, are investigated within the Thomas-Fermi (TF) approximation and full-numerical solution of the corresponding Gross-Pitaevskii (GP) formalism. By comparing the TF predictions with the GP solutions, in our investigation with two different quartic-quadratic trap geometries, of particular relevance is to observe that the TF approach is not only very useful to display the averaged density distribution, but also quite realistic in establishing the critical rotational conditions for the breakup occurrence and possible giant-vortex formation. It provides almost exact results to define the contour of the condensate distribution, even for high rotating systems, after the system split into two (still confined) clouds. The applicability of the Feynman rule to the vortex distribution (full-numerical GP solutions) is also being confirmed for these nonhomogeneous asymmetric trap configurations. This study is expected to be relevant for manipulating the rotation and trap parameters in addition to Feshbach resonance techniques. It can also be helpful to define initial conditions for any further studies on the dynamical evolution of vortex pattern distributions.

DOI: 10.1103/PhysRevA.102.063330

I. INTRODUCTION

The fragmentation phenomenon of objects due to their fast rotation is ubiquitous in physical systems, ranging from classical astronomical objects, such as galaxies and supermassive rotating stars [1–3], to the microscopic world of quantum phenomena, in nuclear physics [4,5]. In atomic-molecular physics, this possibility could also be visualized by considering the experimental realization in Ref. [6] of superfluid flow of quantum gas rotating in an anharmonic potential. Theoretically, the occurrence of breakup in a rotating dipolar condensate was suggested in Ref. [7], when studying three-dimensional (3D) vortex structures in a rotating dipolar Bose-Einstein condensate (BEC). For coupled condensed systems, the breakup can be easily understood as related to the miscibility properties of the mixture, such that the system split into two spatially separated condensates when going to the immiscible regime, in which the rotation can help to reduce the confinement of the two species together [8–14]. With single species atomic condensates, there are plenty of studies with different kind of rotating trap confinements, which allows the generation of multiple quantized vortices, when considering enough strong power-law and anharmonic potentials [15–19]. Among them, of particular interest are the investigations with the more experimentally feasible quartic-quadratic trap combinations [16,17], such that one can identify formations of circular superflow and stable giant vortex, when considering fast and overcritical rotations [20–30]. However, in these cases, without interspecies interaction to play, we are not aware of specific approaches concerning the possibilities to fragment a condensate by introducing high rotation frequencies in a controlled way, with the fragments still kept confined. In this direction, we can foresee the experimental possibilities, which are accessible, as one can follow from the recent studies performed with high rotation superfluids and condensates, generating long-lived dynamical rings [6,31]. In order to generate long-lived stable vortices, the experiments are usually performed with repulsive two-body interactions, as being already well-known that vortices are generally unstable in rotating BEC with attractive interactions [32–35], which are closely related to the condensate requirements for stability [19,36].

In the present work, we consider a BEC with repulsive two-body interactions, as our purpose is to study more closely the possibilities to break a stable condensate by increasing the rotation. For that an originally simple pancakelike two-dimensional (2D) trap confinement is assumed, which is obtained by a much stronger confinement in one of the directions, which can be easily implemented experimentally. Our aim with such study is to fill a gap in the basic literature concerning the properties of rotating BECs [19,36–39], which can be relevant to control and calibrate possible experimental realizations when considering more involved studies on properties of ultra-cold condensed systems. By introducing such a breakup mechanism in an experimental apparatus, with the fragments of the condensate still being kept confined, one could have access to another mechanism to control the condensed cloud, in addition to the Feshbach resonance techniques [40,41]. In view of the above motivations for considering a condensate breakup, we introduce a theoretical

*brito@if.usp.br
†andriati@if.usp.br
‡lauro.tomio@unesp.br
§gammal@if.usp.br

demonstration that such procedure can be easily implemented in a single nondipolar condensate, induced by the rotation in an asymmetric trap. For that, we rely in the Thomas-Fermi (TF) approximation, for a 2D confined system, supported by the corresponding full-numerical results obtained via the usual Gross-Pitaevskii (GP) formalism. The numerical results are performed by imaginary time propagation approach [42] and, complementary, refined by fixed point methods [43].

In order to simplify our analysis and the system be experimentally feasible, we are assuming a strongly confined quasi-2D trap, considering two distinct quartic-quadratic nonsymmetric shapes in the pancakelike perpendicular plane. Both trap nonsymmetric geometries are equally simple to be implemented in actual cold-atom experiments, which are slightly different from the more symmetric quartic-quadratic confinements being so far investigated [17–19,44]. In both the cases that we are studying, a general double-well structure is assumed for the asymmetric confinement, such that just by manipulating the rotation frequency parameter Ω, one can deform and split the condensed cloud in two fragments, which can still be kept strongly confined within fixed two-well positions, which are affected by the Ω value. Of particular relevance for possible experimental proposals, as it will be further discussed, is the outcome of our study on the reliability of the TF approximation, which is quite robust and useful to define the limiting rotational conditions, even for the asymmetric trap structures under analysis, before and after the condensate splits in two fragments.

By full-numerical solution of the GP formalism, we are also investigating the vortex structure patterns, which occur in the two kind of asymmetric quartic-quadratic trap configurations being considered. The applicability of the well-known Feynman rule (FR) [45] in these quite asymmetric geometries is well established, by verifying the vortex density numbers inside the confined condensed cloud, even when applying the rule to each fragment of the condensate, once it is appropriately defined regions with enough vorticity. The role played by hidden vortices (located in low-density regions) is also being characterized in our analysis.

In the next Sec. II, we present some details on the BEC formalism, with quartic-quadratic confinement, in which we are paying particular attention to the related TF description. All the numerical results for the GP formalism, as well as for the TF approach, are presented and discussed along this section, following the formalism. In the Sec. III, we present our analysis on the vortex-pattern distributions verified in the densities, in which we discuss the validity of the well-known Feynman rule for asymmetric shaped BEC confinement. Finally, in Sec. IV, we resume the work with our conclusions and perspectives for further related studies.

II. QUARTIC-QUADRATIC TRAPPED BEC

In the next, we present the usual basic quasi-2D GP formalism, obtained from a 3D reduction to a strongly pancakelike confined system in the x_3 direction. In the formalism two possible trap interactions are being considered in the (x_1, x_2) plane. The breakup conditions are investigated in rotating condensate systems, in which we have verified that the usual TF approximation can successfully describe the density distribution, as well as it is quite helpful in defining the contours of the condensate, before and after the breakup. Therefore, this approximation will be used in order to obtain the necessary rotating frequency in which the fragmentation of the condensate occurs in two parts.

For a condensed system of particles having mass m, confined by a trap potential $V_{3D}(x_1, x_2, x_3) \equiv V_{2D}(x_1, x_2) + m\omega_3^2 x_3^2/2$, where ω_3 is the trap frequency along the x_3 direction, within a rotating frame with angular frequency $\overline{\Omega}$ about x_3, where the angular momentum operator is $L_3 = \mathrm{i}\hbar(x_2\partial/\partial x_1 - x_1\partial/\partial x_2)$, the 2D reduction of the original 3D stationary solution of the modified Gross-Pitaevskii (GP) formalism can be written, for the chemical potential $\mu_2 \equiv \mu_3 - \hbar\omega_3/2$, as

$$\mu_2\psi_{2D} = \left[-\frac{\hbar^2}{2m}\nabla_{2D}^2 + V_{2D} + \overline{\Omega}L_3 + g_{2D}|\psi_{2D}|^2\right]\psi_{2D}, \quad (1)$$

where $\nabla_{2D}^2 \equiv \frac{\partial^2}{\partial x_1^2} + \frac{\partial^2}{\partial x_2^2}$ and $\psi_{2D} \equiv \psi_{2D}(x_1, x_2)$ is the 2D wave function normalized to the number of atoms N (the corresponding density given by $n_{2D} \equiv |\psi_{2D}|^2$), with $V_{2D} \equiv V_{2D}(x_1, x_2)$ being the 2D trap potential. The strength of the nonlinear interaction, g_{2D}, related to the corresponding g_{3D} due to the two-body s-wave interaction a_s, is given by

$$g_{2D} \equiv g_{3D}\sqrt{\frac{m\omega_3}{2\pi\hbar}} \equiv \left(\frac{4\pi\hbar^2 a_s}{m}\right)\sqrt{\frac{m\omega_3}{2\pi\hbar}}. \quad (2)$$

The total energy, related to (1) can be written in terms of the 2D vector $\mathbf{r}$ and its conjugate momentum $\mathbf{p}$, as

$$E[\psi_{2D}] = \int d^2\mathbf{r}\left\{\frac{1}{2m}\psi_{2D}^*(\mathbf{p} - \overline{\mathbf{\Omega}} \times m\mathbf{r})^2\psi_{2D} + \left[V_{2D} - \frac{m\overline{\Omega}^2 r^2}{2}\right]|\psi_{2D}|^2 + \frac{g_{2D}}{2}|\psi_{2D}|^4\right\}. \quad (3)$$

With the energy and length units given, respectively, by $\hbar\omega$ and $l_\omega \equiv \sqrt{\frac{\hbar}{m\omega}}$, we have $(x, y) = (x_1/l_\omega, x_2/l_\omega)$, the GP formalism can be written in dimensionless units. For that, we redefine the respective quantities, appropriately, as $\mu \equiv \mu_2/(\hbar\omega)$, $V \equiv V(x, y) \equiv V_{2D}/(\hbar\omega)$, $\psi \equiv \psi(x, y) \equiv l_\omega\psi_{2D}/\sqrt{N}$, $\Omega \equiv \overline{\Omega}/\omega$, and $L_z = L_3/\hbar$. Therefore, from Eqs. (1)–(3), we obtain the corresponding dimensionless equations, as

$$\mu\psi = \left[-\frac{1}{2}\left(\frac{\partial^2}{\partial x^2} + \frac{\partial^2}{\partial y^2}\right) + V + \Omega L_z + g|\psi|^2\right]\psi, \quad (4)$$

where ψ is normalized to one. In the above, within our units, ω is an arbitrary frequency parameter, which is assumed to be perpendicular to the z direction, with $\lambda \equiv \omega_3/\omega$ being the trap aspect ratio. In this case, the dimensionless nonlinear strength carries the information about the number of atoms N, trap aspect ratio $\lambda \equiv \omega_3/\omega$ and two-body s wave scattering length a_s:

$$g = N\sqrt{8\pi\lambda}\left(\frac{a_s}{l_\omega}\right). \quad (5)$$

We assume repulsive two-body interaction, with $a_s > 0$ throughout this study, due to stability requirements of the

condensate cloud, such that g is always positive. The dimensionless energy, corresponding to (3) is given by

$$\mathcal{E}[\psi] = \int dx\,dy\left\{\frac{1}{2}\left[\left|i\frac{\partial\psi}{\partial x} - \Omega y\psi\right|^2 + \left|i\frac{\partial\psi}{\partial y} + \Omega x\psi\right|^2\right] + \left[V(x,y) - \frac{\Omega^2(x^2+y^2)}{2}\right]|\psi|^2 + \frac{g}{2}|\psi|^4\right\}, \quad (6)$$

from where we can observe that the trap potential is going to be effectively reduced as we increase the rotation frequency. About our full-dimension trap interaction, $V_{3D}(x_1, x_2, x_3)$, as usual we are assuming that the trap aspect ratio $\lambda = \omega_3/\omega$ is large enough in order to validate our quasi-2D geometry approach, in consonance with possible experimental realizations. For that, one can also realize that the number of particles N together with λ and the two-body s wave contact interaction a_s can be conveniently adapted according to the system being investigated, by adjusting the strength g [Eq. (5)].

Within our aim to study the possibility for the rotation frequency to distort up to the breakup of the condensate, let us assume nonsymmetric 2D trap potential in the (x, y) plane, given by a quadratic-quartic interaction. For that, let us fix an harmonic oscillator trap in the y direction, implying $\omega_y = \omega$ in our dimensionless units. For the quartic term, which impose a more strong confinement, we are going to consider two possibilities. The first, just x dependent, with the second more symmetric, exchanging the x^4 by r^4. We can write both trap models as given by

$$V_\sigma(x,y) = \frac{y^2}{2} + \frac{b^2}{4}\left[\left(x^2 - \frac{a^2}{b^2}\right)^2 + \sigma(r^4 - x^4)\right], \quad (7)$$

where $\sigma = 0$ (x quartic) and $\sigma = 1$ (r quartic) define the two kind of traps. In both cases, $b^2/4$ is the strength of the quartic term. The minima for $V_\sigma(x, y)$ are given by $x \equiv \bar{x} = \pm a/b$ and $y = 0$, along x and y directions, respectively.

In the following, we provide a detailed Thomas-Fermi approximation analysis for the density distributions, which will show up to be quite realistic as compared with the numerical results, when used to define the threshold conditions.

A. Thomas-Fermi approximation.

From Eq. (3), we can derive the TF approximation, when the atomic repulsive interactions are dominating, by expanding the condensate to a mean radius that exceeds the mean oscillator length l_ω. In this case, the expansion reduces the radial gradient of the density, with the kinetic energy becoming negligible relative to the trap and interactions, such that

$$\mathcal{E}_{\rm TF}[\psi] \approx \int dx\,dy\left\{\left[V_\sigma(x,y) - \frac{\Omega^2 r^2}{2}\right]|\psi|^2 + \frac{g}{2}|\psi|^4\right\}. \quad (8)$$

By minimizing this energy with respect to $|\psi|^2$ at fixed normalization, we obtain the TF density, which is a function of Ω through $\mu_{\rm TF} \equiv \mu_{\rm TF}(\Omega)$. It is given by

$$n(x,y;\Omega) \equiv |\psi|^2 = \frac{\mu_{\rm TF}}{g} - \frac{1}{g}\left[V_\sigma(x,y) - \frac{\Omega^2 r^2}{2}\right]. \quad (9)$$

We emphasize here that besides the double-well structure provided by V_σ, the centrifugal part effectively enlarge the distance between the minima, as can be seen from the term inside square brackets in the above Eq. (9), where for a fixed Ω, the density $n(x, y; \Omega)$ have two maxima located at $(x, y) = (\pm\sqrt{\frac{\Omega^2 + a^2}{b^2}}, 0)$. In this case, the density at the center of the cloud, given by

$$n_0 \equiv n(0,0;\Omega) \equiv \frac{\mu_{\rm TF} - V_\sigma(0,0)}{g} = \frac{1}{g}\left(\mu_{\rm TF} - \frac{a^4}{4b^2}\right), \quad (10)$$

shall decrease by increasing the rotation, due to centrifugal forces, with the distances between the two density maxima increasing. Within this dynamical process, n_0 can be zero, with the creation of a giant vortex at the center, as well as induce a breakup of the condensate in two clouds, which will depend on the specific trap potential configuration. So, the conditions to occur the breakup, or to generate the giant vortex, are established when the effective chemical potential $\mu_{\rm TF} - a^4/(4b^2)$ becomes zero ($gn_0 = 0$). However, by increasing even more the rotation Ω, the effective chemical potential becomes negative, with gn_0 defined by Eq. (10) representing this effective chemical potential, and not just the density at the center.

For the V_σ traps defined in Eq. (7), the centrifugal contribution can either generate a giant vortex or split the cloud for $\sigma = 1$ (r quartic) case, in contrast to the $\sigma = 0$ (x quartic) case, where the cloud can split as well, but no giant-vortex phase is generated (as it will be shown). Therefore a more relevant criterion is to analyze the contour of the Thomas-Fermi density in polar coordinates, as a function $r(\theta)$, since the breakup can easily be identified with the absence of real solutions at $\theta = \pm\pi/2$ (in view of the maxima distribution along the x direction). In order to support this TF criterion to define the critical rotation conditions for the condensate breakup (both kind of potentials), as well as for the giant-vortex formation (case of r quartic), we rely on the close agreement between the TF approximation with the numerical GP solution when defining the condensate contour. The two trap models defined in Eq. (7), for $\sigma = 0$ (x quartic case) and $\sigma = 1$ (r quartic case), will be treated separately in the next sections.

B. Case of x quartic confinement

The contour of the cloud condensate, obtained by solving $n(x, y; \Omega) = 0$, before and after the breakup, is similar to what is known in mathematics as the *Cassini ovals* [46]. Just at the breakup limit, the corresponding *oval* contour curve can also be identified with the *Bernoulli Lemniscate*. In polar coordinates, with $(x, y) \equiv [x(\theta), y(\theta)] \equiv [r(\theta)\cos\theta, r(\theta)\sin\theta]$, by applying the contour equation $n(x_c, y_c; \Omega) = 0$, we obtain the angular dependence of $r_c \equiv r_c(\theta)$, which is given by

$$4gn_0 = b^2 r_c^4\cos^4\theta - 2r_c^2[(1+a^2)\cos^2\theta - (1-\Omega^2)]. \quad (11)$$

The limit $\theta \to \pi/2$, given by (11), $r_c^2(\pi/2) = 2gn_0/(1-\Omega^2)$, reduces to zero in the breakup, given by Eq. (10),

$$n_0(\Omega_s) = 0 \to \mu_{\rm TF}(\Omega_s) = \frac{a^4}{4b^2}, \quad (12)$$

where Ω_s is the critical rotation frequency to break the condensate in two separated clouds. The above relation expresses

the fact that the chemical potential, which is a general function of the rotation parameter Ω given by Eq. (9), at the breakup (when the density reduces to zero) is given by Ω_s. Therefore the dependence of the breakup condition on the condensate density parameter g can only become explicit once a functional relation becomes established between Ω_s and g, as it will be shown.

The more general solution of Eq. (11), for the contour r_c, is given by

$$b^2 r_{c,\pm}^2 \cos^2\theta = 1 + a^2 - (1-\Omega^2)\sec^2\theta \pm \sqrt{[1 + a^2 - (1-\Omega^2)\sec^2\theta]^2 + 4b^2 g n_0}, \tag{13}$$

where $r_{c,+}(\theta)$ and $r_{c,-}(\theta)$ are the two possible solutions. For $n_0 > 0$, only one solution is possible, $r_{c,+}^2(\theta)$, giving us the full TF contour for $0 \leqslant \theta < 2\pi$. For $n_0 < 0$ (after the breakup), two possible solutions emerge, with $r_{c,-}(\theta)$ corresponding to inner and $r_{c,+}(\theta)$ to outer contour points.

Therefore, aside of Ω_s being the critical rotation for breakup, it is also the threshold minus sign solution for $\Omega > \Omega_s$. Specifically at the critical rotation frequency Ω_s, with $\mu_{\rm TF}$ given by Eq. (12), we have the contour delimited by the + sign solution as

$$r_{c,+}^2(\theta) = 2\frac{\sec^4\theta}{b^2}\left[a^2 + \Omega_s^2 - (1+a^2)\sin^2\theta\right] \times \Theta\left(\frac{a^2+\Omega_s^2}{1+a^2} - \sin^2\theta\right), \tag{14}$$

where $\Theta(\xi)$ is the Heaviside step function (=1 for $\xi \geqslant 0$, =0 for $\xi < 0$). The above implies that, at the critical breakup frequency, the radial contour is limited within a fixed interval. By applying the normalization in Eq. (9), together with (14), after the radial integration, for the given trap parameters a and b, we obtain the relation between the critical splitting rotation Ω_s and the density nonlinear parameter g, which is given by

$$gb^4 = \int_0^{\theta_m} d\theta \cos^4\theta\, r_c^6(\theta) = \frac{32}{105}\sqrt{\frac{(a^2+\Omega_s^2)^7}{1-\Omega_s^2}}, \tag{15}$$

where $\theta_m \equiv \arcsin\left(\sqrt{(a^2+\Omega_s^2)/(1+a^2)}\right) \in [0, \pi/2]$ is fixed by the Heaviside step function in Eq. (14). The parameter g, as defined in (5), is determined by the number of atoms N, the two-body scattering length and the pancake 2D asymmetry λ. Therefore, given g and the trap parameters a and b, we obtain analytically the critical frequency Ω_s for the condensate to split. Within our purpose to verify the effect of a rotation in breaking a condensate, we are obviously considering that the confining asymmetric double-well shaped trap (7) have the parameter ratio a/b such that the two minima position are close enough in order to have a continuous distribution of the condensate when $\Omega = 0$.

In Fig. 1, we are resuming the TF results for Ω_s as a function of gb^4, by considering two indicative fixed values of the parameter a (0 and 0.5). Few sample results for the densities, showing how the rotation is affecting the dynamics of the condensate, are also illustrated in Figs. 2 (with $g = 500$) and 3 (with $g = 2500$), considering numerical GP results. In both the cases, we have $a = 0.5$ and $b = 0.1$, such that the minima

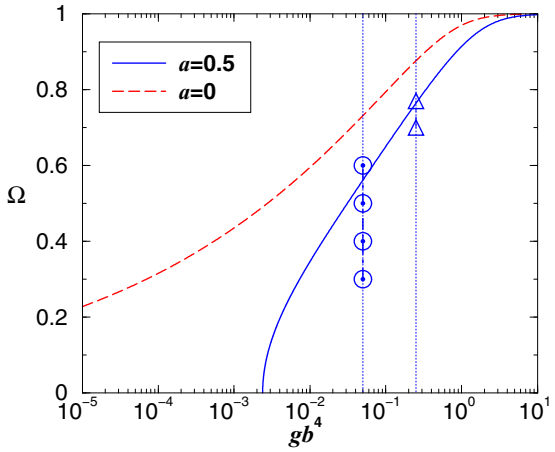

FIG. 1. Rotation frequency Ω as function of gb^4, for the trap defined by Eq. (7), with $\sigma = 0$ and the nonlinear strength g given by Eq. (5). The curves, for $a = 0$ (dashed) and $a = 0.5$ (solid), refer to the TF lower limiting values, Ω_s, to split the condensate. The circles (triangles) are indicating the positions of density-plot illustrations for $a = 0.5$, shown in 4 panels of Fig. 2 (3 panels of Fig. 3), with $gb^4 = 0.05$ ($gb^4 = 0.25$), where $\Omega_s = 0.5616$ (0.7640). With units defined in the text, all parameters are dimensionless.

of the quartic interaction are at $x = \pm 5$. The corresponding parameter positions of these results ($gb^4 = 0.05$ and 0.25, respectively) are also indicated inside the panel of Fig. 1. The corresponding breakup rotational parameter are $\Omega_s = 0.5616$ and 0.7640.

In Fig. 2, we show the numerical GP simulations together with the TF boundaries for the densities, as considering four panels with different arbitrary values of Ω, from 0.3 till 0.6. This figure illustrates how the breakup occurs in a condensate trapped by $V_0(x, y)$ given by Eq. (7), induced by the rotation frequency, which is reducing the strength and shifting the position of the minima of the corresponding effective double-well potential. For a better quantitative analysis, we have also included the panels (e) and (f) corresponding to $|\psi(x, 0)|^2$ of panels (c) and (d). The effective potential related to panel (d) is also being represented in the bottom part of the figure by a surface 3D plot. In particular, we consider remarkable the agreement between the numerical GP computed results with the corresponding TF approximation estimates, when applied to the contour of the condensate (inside which we can find most of the density distributions). Such results obtained by using the TF approximation, as compared with the numerical computed ones, are indicating that it can be quite useful in order to verify the exact rotation frequency Ω_s, at which one should expect the condensate being fragmented in two pieces, once considered fixed the potential parameters. The results presented in the panels (e) and (f) are particularly significant to support the TF approximation in order to define the breakup limiting conditions. In spite of the obvious limitations in describing the vortex pattern structure, the TF approximation provides an averaged good agreement with the numerical GP results for the internal averaged density distributions, remarkably reproducing the corresponding contour borders.

In Table I, the quantitative deviations between the TF and the GP numerical results are verified for the chemical

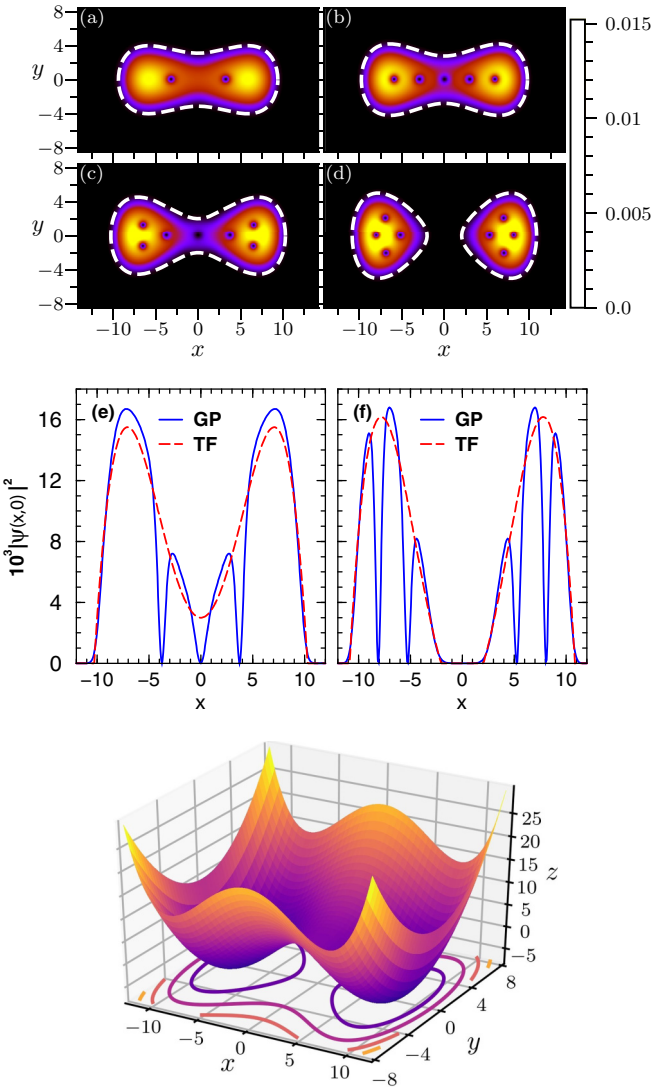

FIG. 2. The densities $|\psi(x, y)|^2$, obtained from the numerical GP solutions, are shown in the upper panels, for $\Omega = 0.3$ (a), 0.4 (b), 0.5 (c), and 0.6 (d), with the TF approximation boundaries represented by white-dashed lines. In (e) and (f), corresponding to $y = 0$ densities (c) and (d), respectively, we compare TF (dashed curves) with GP (solid curves) results. The other parameters are $g = 500$, $b = 0.1$ ($gb^4 = 0.05$), and $a = 0.5$. The effective potential for the panel (d) is illustrated by the surface plot [with $z \equiv V_0(x, y) - 0.18r^2$]. With the defined units, all quantities are dimensionless.

TABLE I. The chemical potentials (GP numerical simulations and TF approximation), for $\Omega = 0$ and the frequencies considered in Fig. 2 are given in this table, together with the corresponding GP Energy values. The units are $\hbar\omega$ for the energy and chemical potentials, with ω for the frequency Ω.

Ω	$\mu_{\rm TF}$	μ	Energy
0.3	5.994	6.469	3.962
0.4	4.813	5.407	2.955
0.5	3.061	3.801	1.271
0.6	0.343	1.215	−1.490

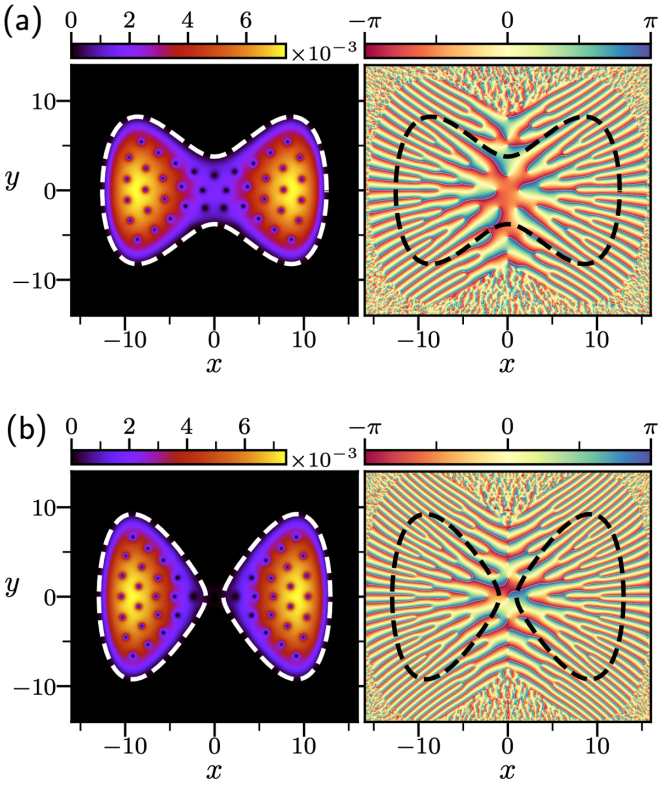

FIG. 3. Density distributions (left) are shown with the corresponding phase diagrams (right), for the nonlinear interaction $g = 2500$ and rotation frequencies $\Omega = 0.7$ (a) and 0.77 (b), whereas the breakup critical value is at $\Omega_s = 0.764$. The trap parameters are the same as in Fig. 2. The TF boundaries are given by dashed lines, with the upper color bars indicating the respective density and phase levels. With the defined units, all quantities are dimensionless.

potentials corresponding to the four specific cases shown in Fig. 2. Among the results, we also add the ones corresponding to the total energy, together with the cases with $\Omega = 0$.

From the GP results shown in Fig. 2, we observe the crescent number of vortices formed inside the condensate as we increase the rotation. The linear increasing behavior of the vortices number with the frequency is clearly being broken near the breakup limit, giving us some indication of the occurrence of possible hidden vortices at the low-density region. This behavior will be further discussed in the next section, within our analysis of vortex pattern distributions.

In order to improve our illustrations of the x quartic confining potential, with densities in which we can verify more clearly how the vortex pattern distributions occur before and after the breakup, we include the Fig. 3, where we consider two specific cases with frequency rotations $\Omega = 0.70$ (a) and 0.77 (b), with the nonlinear parameter, $g = 2500$, which is much larger than in the case of Fig. 2. However, in both the cases, we are keeping the same trap parameters, $a = 0.5$ and $b = 0.1$, with the potential minima at $x = \pm 5$. These plots, in which a richer pattern structure can be observed, were obtained by the GP numerical simulations for the densities (left panels), with the corresponding phase diagrams (right panels). The boundary definitions, indicated inside the panels, were obtained by using the TF approximation. As shown in

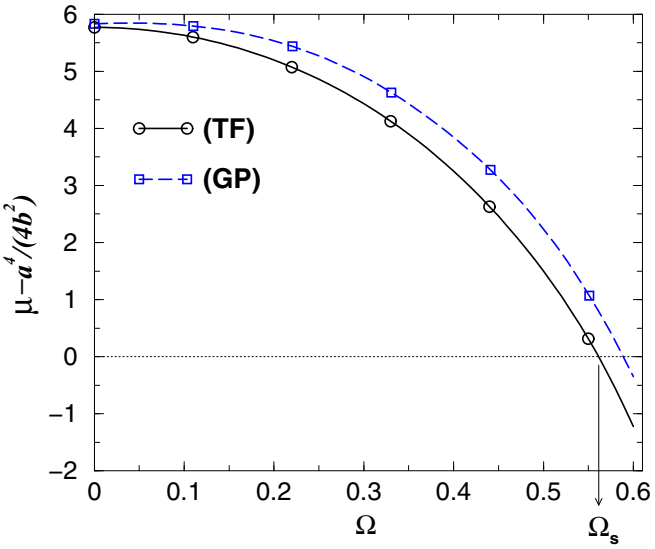

FIG. 4. The dependence of the effective chemical potentials [GP and TF results], given by $\mu - a^4/(4b^2)$, on the rotation frequency Ω for the trap parameters $a = 0.5$ and $b = 0.1$. The TF (GP) results are indicated, respectively, by the circles (squares), being fitted by solid (dashed) lines. At $\Omega = 0$, $\mu_0 = 7.332$ (TF) and 7.395 (GP). For zero density, when $\mu = (5/4)^2$, we obtain $\Omega_s = 0.5616$, within the TF approximation; and 0.590 within the GP result. With the given units, all quantities are dimensionless.

the panel (b), with rotation frequency $\Omega = 0.77$, the condensate is already broken in two fragments. Due to the rotation $\Omega = 0.77$, the positions of the minima of the effective potential move to $x = \pm 9.18$, with both fragments presenting about the same kind of triangle vortex pattern distributions. As for $\Omega = 0.70$, panel (a), we observe about the same vortex pattern, with the minima of the effective potential being at $x = \pm 9$. In both phase diagrams, we observe the existence of hidden vortices which are located in the low-density regions, along the y axis, close to $x = 0$. More specifically, these hidden vortices are located outside the region defined by the TF approximation, as they are manifested only by solving the full GP formalism.

By considering the same potential parameters used in Table I and in Fig. 2, with $a = 0.5$ and $b = 0.1$, we also present in Fig. 4 the corresponding behavior of the effective chemical potential, given by $\mu - a^4/(4b^2)$, in terms of the rotation frequency Ω, which is zero at the condensate breakup, when $\Omega = \Omega_s = 0.5616$. For that we consider the TF approximation results together with numerical solutions obtained from the GP equation. The results can be well fitted by approximate analytical polynomial expressions. From these analytical results, we observe the quite small deviation of the TF critical breakup rotation limits, $\Delta\Omega_s = 0.028$. We also observe that the deviation of the TF chemical potential $\mu_{\rm TF}$, from the GP values μ becomes larger for fast rotations, which one could expect due to the fact that, by increasing the rotation, more vortices are emerging in the condensate, with the effective confining interaction being diminished in comparison with the kinetic energy term. This is evidenced by the density plots shown in Fig. 2.

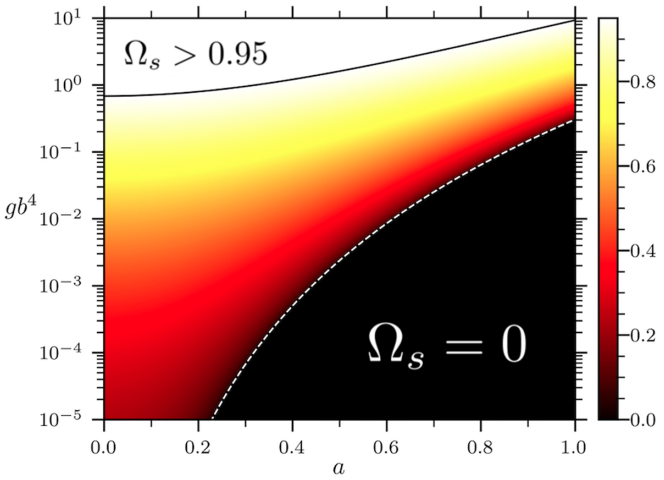

FIG. 5. For the x quartic trap potential [Eq.(7) with $\sigma = 0$], we show by a color-level map (indicating the necessary split frequency Ω_s) the corresponding parametric region for which a rotation is required for breaking the cloud. The upper white region corresponds to $\Omega_s > 0.95$ at which the condensate is likely to fly apart in the y direction before the split occurrence. Below the white-dashed line ($\Omega_s = 0$), the cloud is already spatially separated by the two-well shaped trap. With given units, all quantities are dimensionless.

In Fig. 5, a diagrammatic picture shows the relation between the trap parameters gb^4 and a for the x quartic potential [Eq. (7) with $\sigma = 0$], indicating the necessary rotation Ω_s to split the condensate. Ω_s is represented by the color density, considering the upper-white region $\Omega_s > 0.95$ the region at which the condensate likely flies apart before the breakup. The parameter region at which the condensate is already broken by the potential parameters is shown below the dashed line (where $\Omega_s = 0$).

C. Case of *r* quartic confinement

By considering the confining potential given by Eq. (7) with $\sigma = 1$, we have a trap with quadratic+quartic radial symmetry in the (x, y) plane, with the symmetry broken in the x direction, which can be written as

$$V_1(x, y) = \frac{r^2}{2} + \frac{b^2}{4}r^4 - (1 + a^2)\frac{x^2}{2} + \frac{a^4}{4b^2}, \qquad (16)$$

Different from the previous x quartic trap, in this case we have also a quartic component in the y direction. The $|x|$ and $|y|$ extreme limits for nonzero density, obtained by using the Eq. (9) are defined by

$$n(x, y) \equiv |\psi|^2 = \frac{\mu_{\rm TF}}{g} - \frac{1}{g}\left[V(x, y) - \frac{\Omega^2 r^2}{2}\right]$$
$$= n_0 - \frac{1}{2g}\left(y^2 - a^2x^2 + \frac{b^2}{2}r^4 - \Omega^2 r^2\right), \qquad (17)$$

where $gn_0 \equiv [\mu_{\rm TF} - a^4/(4b^2)]$ as also given by Eq. (10). Analogously as in the x quartic case, we could follow by using polar coordinates. However, before that, it may be useful to verify the extremes of nonzero density $n \equiv n(x, y)$. So, by deriving in the x coordinate, we can identify a minimum at

$x = x_0 = 0$ with two maxima at $x = x_\pm$ of (17), given by

$$x_\pm = \pm\sqrt{\frac{\Omega^2 + a^2}{b^2} - y^2}, \quad x_0 = 0. \tag{18}$$

Similarly, by deriving in the y coordinate (given x), we can identify the existence of two maxima at $y = y_\pm$ with a minimum at $y = y_0 = 0$, only when $\Omega^2 > 1 + b^2x^2$,

$$y_\pm = \pm\sqrt{\frac{\Omega^2 - 1}{b^2} - x^2}, \quad y_0 = 0. \tag{19}$$

Combining both results, we verify that for $\Omega^2 > 1$ we can have extrema (two maxima and one minimum) only in the x direction, located at $(x_\pm, 0)$ ($\theta = 0$), as the maxima obtained by (19) are located outside the positions where the previously broken condensate parts are located, as we can see by replacing $x_\pm^2$ in (19).

Now, let us consider the density contour given by Eq. (17) in polar coordinates, $(x, y) \equiv [x(\theta), y(\theta)] \equiv [r(\theta)\cos\theta, r(\theta)\sin(\theta)]$, such that $r_c \equiv r_c(\theta)$ is given by

$$4gn_0 = b^2r_c^4 - 2r_c^2[(1 + a^2)\cos^2\theta - (1 - \Omega^2)], \tag{20}$$

$$b^2r_c^2 = (1 + a^2)\cos^2\theta - (1 - \Omega^2) \pm \sqrt{[(1 + a^2)\cos^2\theta - (1 - \Omega^2)]^2 + 4b^2gn_0}. \tag{21}$$

We should emphasize that the necessary and sufficient condition for the breakup is that no real solution occurs for $r_c^2(\pm\pi/2) \equiv y_c^2$ (implying density zero along the y axis, not only at $y = y_c$). In the x quartic case ($\sigma = 0$), the $n_0 = 0$ condition is enough for the breakup, with the frequency being limited to $\Omega \leqslant 1$, as shown. Nevertheless, differently from x quartic case, as we take $\theta = \pm\pi/2$ in Eq. (20) we still end up with a biquadratic equation for the radius, with the Eq. (21) simplified as

$$b^2y_c^2 = (\Omega^2 - 1) \pm \sqrt{(\Omega^2 - 1)^2 + 4b^2\left[\mu_{\rm TF} - \left(\frac{a^4}{4b^2}\right)\right]}. \tag{22}$$

The existence of solutions for this equations implies that, at $\theta = \pm\pi/2$, the contour is connected. So, next we consider all the possibilities in (22), where $gn_0 = \mu_{\rm TF} - a^4/(4b^2)$. If $gn_0 > 0$ only the $+$ sign solution can exist, corresponding to a connected contour in the TF description. However, if $gn_0 \leqslant 0$, the existence of real solutions (characterizing contour connected) depends on Ω: For $\Omega < 1$, neither the $+$ nor the $-$ solutions are possible, characterizing the breakup of the cloud. However, for $\Omega > 1$, both solutions are possible, if $0 > 4b^2gn_0 > -(\Omega^2 - 1)^2$, corresponding to the upper and lower solutions of the connected contour, which is identifying the giant-vortex formation at the center. The other possibility, when $4b^2gn_0 < -(\Omega^2 - 1)^2$, there is no real solution for Eq. (22), which will corresponds to the breakup. Summarizing:

$\Omega > 1$	$-(\Omega^2 - 1)^2 < 4b^2gn_0 \leqslant 0$	Giant vortex
	$-(\Omega^2 - 1)^2 \geqslant 4b^2gn_0$	Breakup
$\Omega \leqslant 1$	$gn_0(\Omega) \leqslant 0$	Breakup

(23)

The critical values for the rotation parameter Ω are corresponding to the transitions among the phases, which are obtained when the equality holds in the above relations, being defined as Ω_G for the Giant-vortex formation (which can happen only for $\Omega > 1$), and Ω_s the critical frequency to split the cloud.

Differently from the first trap studied, in the one defined by Eq. (16), the breakup regime can be achieved for larger values of b since the condensate will no longer fly apart due to the presence of quartic confinement also in the y direction.

In the above, we have considered the possible breakup of the condensate (as well as the giant-vortex formation in the origin) along the y axis (considering $\theta = \pm\pi/2$, or $x = 0$), when by increasing the rotation (with $\Omega > 1$) the quadratic confinement in the y direction is reduced till the condensate split into two fragments. However, a similar situation could occur in the x direction, if the asymmetry of the trap potential which is holding the two fragments can allow minima for the density at $y = 0$ ($\theta = 0$) for fixed values of $\pm x$, in Eq. (21). This should be given by the following second-order equation:

$$b^2x_c^2 = (\Omega^2 + a^2) \pm \sqrt{(\Omega^2 + a^2)^2 + 4b^2gn_0(\Omega)}. \tag{24}$$

For larger values of Ω^2 ($\gg a^2$), the Eqs. (22) and (24) provide the same results for y_c and x_c, respectively.

In the following, let us first consider $n_0(\Omega) = 0$ in Eq. (21), which give us a critical Ω_c. This is the split critical frequency Ω_s for $\Omega \leqslant 1$. However, for $\Omega \geqslant 1$, it is a critical rotation for a giant vortex to appear, such that $\Omega = \Omega_G$. For $n_0(\Omega_c) = 0$, the critical condition gives

$$r_c^2(\theta) = \frac{2(1 + a^2)}{b^2}[C(\Omega_c) - \sin^2\theta]\Theta(C - \sin^2\theta),$$

with

$$C \equiv C(\Omega_c) \equiv \frac{a^2 + \Omega_c^2}{1 + a^2}. \tag{25}$$

In the above, the Heaviside step function is only effective in case $\Omega_c \leqslant 1$, when C can define an upper limit for the angle θ, given by θ_m. In such a case, we can assume $C \equiv \sin^2\theta_m$ for $\Omega_c \leqslant 1$. In the other case, for $\Omega_c \geqslant 1$, we keep C as defined in Eq. (25).

By applying the normalization condition in Eq. (17), together with Eqs. (20) and (25), we obtain

$$\begin{aligned} gb^4 &= \frac{b^6}{24}\int_0^\pi d\theta r_c^6 \\ &= \Theta(1 - \Omega)\frac{2(1 + a^2)^3}{3}\int_0^{\theta_m} d\theta[C - \sin^2\theta]^3 \\ &\quad + \Theta(\Omega - 1)\frac{2(1 + a^2)^3}{3}\int_0^{\pi/2} d\theta[C - \sin^2\theta]^3 \\ &= \frac{(1 + a^2)^3}{48}\Big\{-(2\theta_m)\cos(2\theta_m)[2\cos^2(2\theta_m) + 3] \\ &\quad + \frac{\pi(1 + a^2)^3}{3}\left\{\left(C - \frac{1}{2}\right)\left[C^2 - C + \frac{5}{8}\right]\right\}\Theta(\Omega - 1). \\ &\quad + \left[\left(5 - \frac{11}{3}\sin^2(2\theta_m)\right)\sin(2\theta_m)\right]\Big\}\Theta(1 - \Omega)e \end{aligned} \tag{26}$$

In the first case ($\Omega \leqslant 1$), when the integral is limited by θ_m, we can identify Ω_c with the critical splitting frequency Ω_s. And, in the second case, for $\Omega \geqslant 1$, the upper limit of the integral is fixed at $\pi/2$, with the critical value corresponding to the creation of a *giant vortex*, such that we identify Ω_c with Ω_G, which is within the definition of C, given in Eq. (25). Therefore, in the above, we have $C \equiv (a^2 + \Omega_G^2)/(1 + a^2)$.

Some specific cases: (i) with $\Omega^2 \leqslant 1$, we notice that in the nonrotating case $\Omega = 0$, for $a^2 = 1$, we obtain $gb^4 = 2/9$; and (ii) with $\Omega \geqslant 1$, for the giant-vortex critical frequency, when $\Omega_G^2 = 1$, we obtain $gb^4 = 5\pi(1 + a^2)^3/48$ (= 0.639, if $a = 1/2$); and with $\Omega_G = 2$, $gb^4 = 52.11$ (with $a = 1/2$) and 46.27 (with $a = 0$).

Next, we consider the breakup for the second case, $\Omega^2 \geqslant 1$, which is obtained by increasing the rotation frequency beyond Ω_G, till the condensate split into two fragments. So, the density at $x = 0$ (for any value of y), which is given by

$$n(0, y) \equiv \frac{1}{g}\left[\left(\mu_{\rm TF} - \frac{a^4}{4b^2}\right) - \frac{b^2}{4}y^4 - \frac{1 - \Omega^2}{2}y^2\right], \quad (27)$$

becomes zero along the y axis, at a critical frequency $\Omega = \Omega_s > \Omega_G$, when $gn(0, y) = 0$. This condition is expressed by $4b^2 gn_0 = -(\Omega_s^2 - 1)^2$ in (23), implying in $b^2 y_c^2 = (\Omega_s^2 - 1)$ at the critical breakup limit. Next, by following the same procedure as before, we consider the corresponding contour $r_c(\theta)$. By applying the normalization (17), we obtain

$$\begin{aligned} gb^4 &\equiv \frac{2}{3}(1 + a^2)^3 \int_0^{\pi/2} d\theta \cos^3\theta \\ &\quad \times \sqrt{\left[\frac{2\Omega^2 + a^2 - 1}{a^2 + 1} - \sin^2\theta\right]^3} \\ &= \frac{2(1 + a^2)^3}{3} \int_0^1 dz(1 - z^2)[\zeta^2 + 1 - z^2]^{3/2}\big|_{\zeta^2 \equiv \frac{2(\Omega^2 - 1)}{a^2 + 1}} \\ &= \frac{(1 + a^2)^3}{72}[\zeta(3\zeta^4 + 22\zeta^2 + 15) \\ &\quad - 3(\zeta^2 - 5)(\zeta^2 + 1)^2 \cot^{-1}\zeta]. \end{aligned} \quad (28)$$

Therefore, in case $\Omega^2 = 1$, we have $\zeta = 0$, with $gb^4 = 5\pi(1 + a^2)^3/48$, in agreement with the previous result we have obtained for $\Omega^2 \leqslant 1$.

With Fig. 6 we resume our results for the critical frequencies in terms of gb^4, considering two values for the parameter a (=0 and 0.5). For a better display of the lower rotation frequency, $\Omega < 1$, the results are presented in a logarithmic scale in the inset. For such cases with $\Omega < 1$, we can only observe breakup of the condensate, with the limiting condition Ω_c given when the density at the center reduces to zero. To illustrate this case, we have the density distribution of the condensate shown in Fig. 7, where we include three panels with sample results, obtained by the numerical GP results. With $\Omega = 0.6$ [panel (a), before the breakup], $\Omega = 0.75$ [panel (b), close to the breakup], and $\Omega = 0.85$ [panel (c), after the breakup]. To further appreciate the utility of the TF approximation for the analysis of the radial-quartic trap confinement, we are also including the Fig. 8 with several panels, in which the upper panels [(a), (b) and (c)], with $\Omega^2 < 1$, are in agreement with the same numerical results already presented

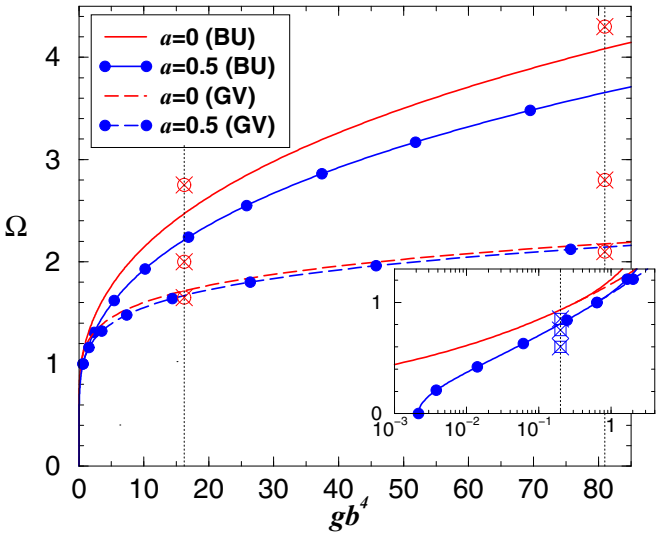

FIG. 6. The condensate critical frequencies Ω to originate the giant vortex (Ω_G) (GV, dashed lines) and for the breakup (Ω_s) (BU, solid lines) for $a = 0$ and $a = 0.5$ (line with bullets). The crossed-circles are indicating the coordinate positions of density plots shown in the three panels of Fig. 9 and also for the density plots given in the three lower panels of Fig. 8 (indicated by the dotted lines at $gb^4 = 16.2$ and 81, respectively). The inset (in log scale) shows the corresponding behavior for lower $\Omega < 1$, with the crossed-squares indicating the coordinate positions of the density plots shown in the upper panels of Fig. 8 (indicated by the dotted line at $gb^4 = 0.2$). With the defined units, all quantities are dimensionless.

in Fig. 7 (parameters $a = 0.5$, $b^2 = 0.02$ and $g = 500$). As also indicated in Fig. 6, no giant vortex can be formed for these low-rotation frequency cases, but just breakup is possible. In the lower panels of Fig. 8, we have also TF results with $\Omega^2 > 1$, corresponding to potential parameters given by $a = 0$, $b^2 = 0.18$ and g=2500, for $\Omega = 2.1$ [(d), just below the formation of a giant vortex], 2.8 [(e), after the giant vortex is formed] and 4.3 [(f), after the breakup]. All these cases are indicated in the Fig. 6; with gb^4 given in a logarithmic-scale inset panel for lower frequencies, and with gb^4 in normal scale shown in the main panel for higher frequencies.

When considering higher frequencies, $\Omega > 1$, as we increase Ω (for given potential parameter), we first observe a giant vortex being created at the center, for which the limiting Ω is identified by Ω_G, represented in Fig. 6 by the dashed

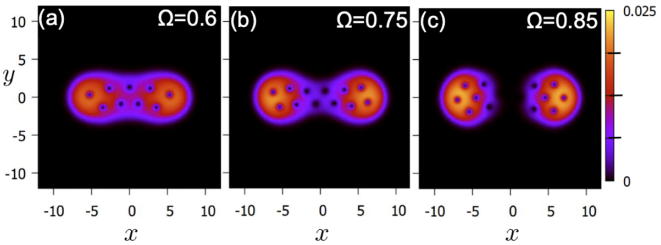

FIG. 7. For r quartic potential [Eq (16)], with $g = 500$, $a = 0.5$, and $b^2 = 0.02$ ($gb^4 = 0.2$), these three panels, for $\Omega = 0.6$ (a), 0.75 (b), and 0.85 (c), are exemplifying the density profiles corresponding, respectively, to low frequency conditions, before, close to, and after the breakup. With the defined units, all quantities are dimensionless.

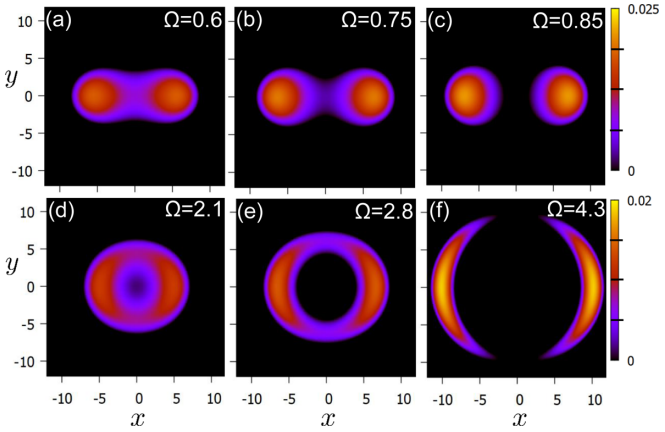

FIG. 8. Densities by using the TF approximation, for the r quartic potential. The upper panels are for low frequencies, as in Fig. 7, with $g = 500$, $a = 0.5$, and $b^2 = 0.02$ ($gb^4 = 0.2$). The lower panels are for high frequencies, when giant vortex and breakup can be verified, with $g = 2500$, $a = 0$, and $b^2 = 0.18$ ($gb^4 = 81$). The values of Ω are indicated inside the panels. With the defined units, all quantities are dimensionless.

lines. In order to verify the splitting of the cloud, we need to increase Ω, even more, such that $\Omega_G < \Omega$, with the limiting given by Ω_s, represented in Fig. 6 by the solid lines. This case with $\Omega > 1$ is also illustrated with three panels in Fig. 9, for $\Omega = 1.65$ [panel (a), before the giant vortex is created], $\Omega = 2$ [panel (b), where we observe the giant vortex at the center, before the breakup], and $\Omega = 2.75$ [panel (c), after the breakup]. In these three panels, we also show that the TF approximation can give quite precisely the contour of the cloud, along all the stages of the rotation-frequency conditions; namely, before the creation of the giant vortex, during and after that, and even after the cloud is fragmented in two parts. We are also illustrating this figure with a 3D surface representation of the effective potential, corresponding to the panel (c).

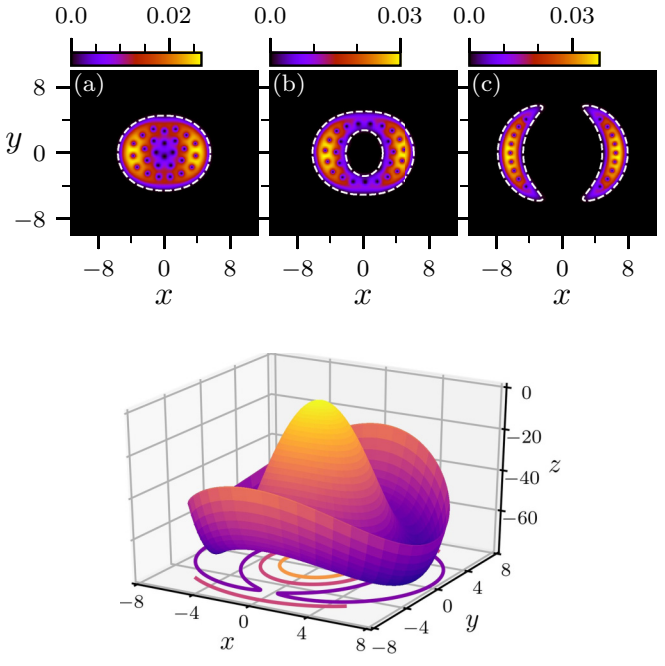

FIG. 9. The upper panels show $|\psi|^2$, by using the Eq. (16), with $g = 500$, $b^2 = 0.18$ ($gb^4 = 16.2$) and $a = 0$, considering $\Omega = 1.65$ (a), 2.00 (b), and 2.75 (c). These panels are exemplifying specific points of Fig. 6, with giant hole in (b) and after the breakup, in (c). The TF contour are shown by the white-dashed lines, obtained as solution of Eq. (21). The surface plot shows the effective potential corresponding to panel (c) [$z \equiv V_1(x, y) - (2.75)^2/2$]. With the defined units, all quantities are dimensionless.

In Fig. 9, the panels (a), (b), and (c) refer to the three points shown in Fig. 6 with $gb^4 = 16.2$. One may clearly note the centered-hole phase in Fig. 9(b) and the breakup in Fig. 9(c). Corresponding to the three specific cases shown in Fig. 9, together with the no-rotating case, in Table II we have the TF and GP chemical potentials, with the GP total energy.

In view that it was clearly shown that the TF approximation works quite well to define the contour of the condensate, as shown in the three panels of Fig. 9, we found useful also to verify the effect of increasing the density factor from $g = 500$ to 2500, by considering the panel (c) of Fig. 9. For that, in Fig. 10, we kept the same values gb^4 used in Fig. 9, with $a = 0$ and $\Omega = 2.75$. As shown, a length-scale transformation is observed, which is also reflected in the corresponding density. The length-scale transformation is transparent in the Eqs. (17)–(19). As one can see clearly, we have a scale transformation, such that $(\tilde{x}, \tilde{y}) = (bx, by)$ implies $gn(x, y) \to [gb^2\tilde{n}(\tilde{x}, \tilde{y})]$ (with $\int d\tilde{x}d\tilde{y}\,\tilde{n}(\tilde{x}, \tilde{y}) = 1$).

By considering this scaling transformation, it is possible to be verified that both results, shown in Figs. 9(c) and 10, will correspond to the scaling of all the corresponding physical quantities, as the trap interaction, chemical potential and energies (which will be multiplied by a factor b^2). Within this scaling procedure, the strength of the nonlinear term will be rescaled, such that $g \to \bar{g} = gb^4$. Therefore the net effect due to the kinetic energy, which is obtained by solving the full GP formalism, will be reflected on the relation of this energy with the frequency parameter Ω, with the increasing vorticity of the system.

Another aspect which may be of interest, is to estimate numerically the free expansion of the condensate, by switching off the trap, in order to check with possible experimental realizations. By considering a limited short time interval, with $t < 16$ (units ω^{-1}), we have verified that the vortex patterns and corresponding numbers are kept about the same during the expansion, when considering a case with high frequency in which a giant vortex can be observed at the center. As expected, the density starts being reduced as the condensed cloud expands, with the size of the giant vortex increasing

TABLE II. The chemical potentials (GP numerical results and TF approximation), for $\Omega = 0$ and for the three cases presented in Fig. 9, are shown in this table. The units are $\hbar\omega$ for the energy and chemical potentials, and ω for Ω.

Ω	μ	$\mu_{\rm TF}$	Energy
0	15.787	15.637	9.814
1.65	3.808	1.484	−0.199
2	−6.082	−8.922	−10.274
2.75	−52.490	−62.741	−57.417

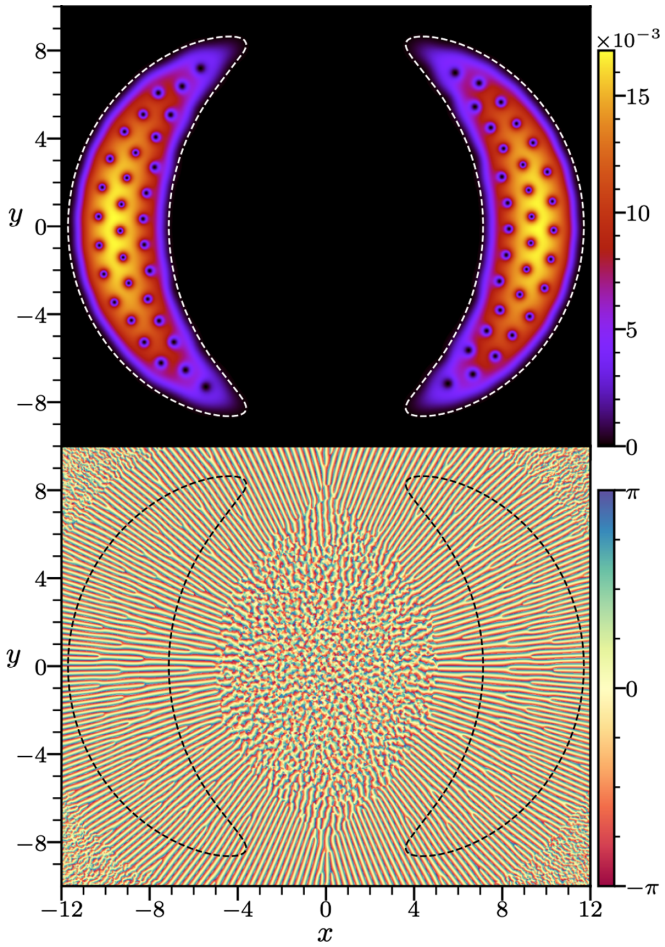

FIG. 10. The density with vortex distributions (top), together with the corresponding phase diagram (bottom), are shown for $g = 2500$, with $a = 0$, $gb^4 = 16.2$, and $\Omega = 2.75$, as in Fig. 9(c) [implying $b^2 \approx 0.08$]. The results are from numerical GP equation, with the dashed contour lines given by the TF approximation. With the defined units, all quantities are dimensionless.

at the same proportion. However, we understand that the required time period for numerical simulations should be much larger, covering an increasing spatial distribution, in order to draw a more conclusive picture about this dynamics, such that could be more useful for experimental studies. This is a perspective theoretical investigation of great interest to be performed within a full dynamical study in which one could introduce time-dependent parameters in the trap interaction.

III. VORTEX PATTERN DISTRIBUTION AND THE FEYNMAN RULE

As observed from the numerical results, the vortex pattern distribution follows approximately the corresponding space occupied by the condensate cloud. The number of vortex is related to the angular frequency of the rotation and the space occupied by a rotating superfluid, which is the well-known Feynman rule (FR) [45] established when studying the liquid helium (For a detailed analysis, considering rapidly rotating condensate with dense array of vortices, see Ref. [19]). According to this rule, the number of vortices N_v inside a given area A is linearly proportional to the rotation frequency Ω, which in our dimensionless units can be written as $N_v = \Omega A/\pi$. As pointed out in Ref. [47], this rule was initially formulated for uniform superfluid helium, been intensively studied both theoretically and experimentally for a BEC trapped in a single harmonic potential. So, it is of interest to verify the extension of the rule when considering trap geometries other than symmetric ones. In our case, by considering the results shown in Fig. 2, we noticed that apparently it fails if we consider the visible vortices within the full area defined by the TF boundaries. However, one should realize that may not be the correct way to apply the rule, in particular when the area is not regular, having low-density regions, such that the visible vortex distribution becomes not uniform. In this regards, the discrepancy in the applicability of the FR has been observed before for the case of double-well trap confinement [47], being attributed to hidden vortices.

In order to clarify that, let us first consider the cases represented in Fig. 3, where the nonlinear term is much larger than in Fig. 2, with $g = 2500$. Notice that, after the breakup, when $\Omega = 0.77$ [panel (b)], the densities of the two fragments are more or less established visibly within two triangle formats, if one considers the limiting space defined by the TF contours. In this case, we can visually approximate the total area as the corresponding one occupied by two triangles, having $A = 2 \times 90$ (units of l_ω^2). With that, by applying the FR just for the visible vortices, we obtain $N_v \approx 0.77 \times (180/\pi) \approx 44$, which matches exactly with the observed visible vortices inside the area defined by the TF boundary. In the other case, before the breakup, shown by the panel (a) of Fig. 3, with $\Omega = 0.7$, we have 41 visible vortices inside the TF contour limits, also in accordance with the corresponding FR prediction. So, the assumption presented in Ref. [47], as requiring hidden vortices to enter in the estimated value of N_v, apparently fails when considering these specific results. Let us try to clarify that. By considering the respective phase diagrams for the panels (a) and (b), we can clearly verify the existence of hidden vortices in the low-density regions (see, in particular near the $x = 0$ positions). However, they are outside the area defined by the TF contour, where we are applying the Feynman rule. More precisely, they are emerging only when we consider a more extended area for the densities, which is given by the GP numerical solution. So, once consistently we define the respective area in which enough vortices exist, the applicability of the FR is observed. Suppose, for instance, that we ignore the TF limiting space, considering a circular area with center at $(x, y) = 0$ and arbitrary radius, covering a space such that we include the hidden vortices near $x = 0$. Again we could verify, approximately, the applicability of the Feynman rule; this time, including the hidden vortices.

In resume, the possible regularity of the trap can only be used to explain visual discrepancy in the applicability of the FR if, inside the given specific region there are hidden vortices, which need to be included. In Figs. 2 and 3, we have about the same confining potential shape. So, for small nonlinearity, as with $g = 500$, the rule apparently is requiring hidden vortices to be verified (present inside the TF limiting contour), but not in the second case. In conclusion, the visual verification of the FR in a large area requires an enough dense cloud, which can support larger number of vortices, as

TABLE III. Applicability of the Feynman rule in the given examples of this contribution, Figs. 2–10. $2R_m$ is the predicted distance between two vortices. D is a visual approximate distance between the closest vortices (extracted near the minima of the effective potential, with possible ± 0.04 error).

Fig.	*Panels*	Ω	$2R_m$	D	g
2	(a)	0.3	3.65	([a])	500
	(b)	0.4	3.16	3.00	500
	(c)	0.5	2.83	2.60	500
	(d)	0.6	2.58	2.40	500
3	(a)	0.70	2.39	2.40	2500
	(b)	0.77	2.28	2.30	2500
7	(a)	0.60	2.58	2.50	500
	(b)	0.75	2.31	2.25	500
	(c)	0.85	2.17	2.00	500
9	(a)	1.65	1.56	1.46	500
	(b)	2.00	1.41	1.37	500
	(c)	2.75	1.21	1.09	500
10	-	2.75	1.21	1.20	2500

[a]Not applicable, as we have only one vortex near each minimum.

in the second case, when we have the nonlinear parameter $g = 2500$ (indicating larger condensed cloud). With enough dense cloud, one can select an arbitrary specific area inside the condensate to apply the rule.

By considering a minimum area $A = \pi R_m^2$ to have one vortex inside, the rule can be expressed by

$$\eta_v \equiv \frac{N_v}{A} = \frac{\Omega}{\pi}, \quad \rightarrow \quad R_m = \sqrt{\frac{1}{\Omega}}, \tag{29}$$

which also implies in about $2R_m$ the distance between two vortices. From this reading, the FR can be approximately verified, not only for the case that we have a condensate enough dense with $g = 2500$ (where we have verified complete agreement), but even for the case that we have $g = 500$, shown in Fig. 2. This is shown by the Table III, where R_m comes from Eq. (29), with D obtained visually from the respective panels. In this way, the applicability of the FR can also be extended by including low-density regions, where regular patterns of hidden vortices can be detected, by examining the corresponding phase diagrams. See, for example, the results shown in the Fig. 10, in which hidden vortices (not visible in the upper panel) can be identified (outside the TF contour line) in the corresponding phase diagram.

IV. CONCLUSIONS

The parameter conditions for a single ultra-cold rotating Bose-Einstein condensate to be fragmented, as well as to form giant vortex at the center, were investigated in this work, by using two kinds of asymmetric pancakelike external quartic-quadratic potentials. The corresponding GP formalism was solved by numerical approach, as well as by a detailed analysis using the TF approximation. The computational results were obtained for low and high rotational frequencies, describing the usual vortex-pattern distributions. In this case, the vortex density distributions was found to follow closely the well-known Feynman rule, once we have appropriately defined the specific region where enough vortices can be observed.

Of particular relevance, considering that it can be quite useful in experimental setup analysis, is TF approximation reliability to define the limiting frequencies for the density distribution of the condensate, even when considering the quite nonuniform condensate distributions. The space contour limits of the condensate, as well as the averaged density distributions, are shown to be well described by the TF approximation, as compared with the GP numerical results, even after the breakup of the condensate, which happens as the rotation frequency increases. These results, verified for different quartic-quadratic confinement, and also by varying the repulsive interaction parameter, provides some further support to the TF approximation even when considering single atomic systems with more complex properties.

As expected, the vortex pattern picture is provided by the GP numerical approach, in which we noticed a quite regular triangular shape structure for the vortices, when the rotation is enough high, before the condensate breakup. The vortex distributions, close to their symmetrically distributed maxima (minima of the effective potential), apparently are not strongly affected by the breakup conditions when higher rotation are implemented. In these cases, we have also verified that the visible vortex pattern distributions follow the well-known Feynman rule, when applying this rule for sample spacial region with enough number of vortices. With this rule given in terms of the vortex density, we can define a unit of area in order to apply the FR even to low-density regions, where hidden vortices are more likely to appear.

The present study for the breakup conditions in rotating condensate was done for the simplest possible situation in which we consider an asymmetric quartic-quadratic trap confinement, enough large to control possible higher rotation conditions, in which the condensate fragments are still kept confined. The possible relevance of the present investigation relies in the fact that we are providing quite well defined limiting conditions via TF approximation (to our acknowledgment, not presented before in the usual literature), which can be easily followed in actual experimental realizations, with different condensed atomic samples, trapped in quartic-quadratic pancakelike potentials.

We understand this kind of study can be quite useful particularly when designing experimental setups of other more involved investigations, such as with dipolar single-component BEC systems, binary miscible and immiscible combinations, etc. As a perspective interesting study, one could further investigate the confined system by assuming time-dependent rotation frequency or trap configurations, which could be introduced by using the present approach. By manipulating the trap configuration as shown, for example, in this work, one could implement another mechanism to control the condensed cloud, in addition to the use of Feshbach resonance techniques.

ACKNOWLEDGMENTS

We are grateful to R. Dubessy for his interest and helpful discussion. The authors thank the Brazilian agen-

cies Fundação de Amparo à Pesquisa do Estado de São Paulo (FAPESP) [Contracts No. 2018/02737-4 (A.A.), No. 2017/05660-0 (L.T.), and No. 2016/17612-7 (A.G.)], Conselho Nacional de Desenvolvimento Científico e Tecnológico [Procedures No. 304469-2019-0 (L.T.) and No. 306920/2018-2 (A.G.)] and Coordenação de Aperfeiçoamento de Pessoal de Nível Superior [Procedure No. 88887.374855/2019-00 (L.B.)].

[1] A. Maeder, *Physics, Formation and Evolution of Rotating Stars* (Springer, Berlin, 2009).

[2] H. Uchida, M. Shibata, T. Yoshida, Y. Sekiguchi, Yuichiro, and H. Umeda, Gravitational collapse of rotating supermassive stars including nuclear burning effects, Phys. Rev. D **96**, 083016 (2017).

[3] C. Chiappini, U. Frischknecht, G. Meynet, R. Hirschi, B. Barbuy, M. Pignatari, T. Decressin, and A. Maeder, Imprints of fast-rotating massive stars in the galactic bulge, Nature (London) **472**, 454 (2011).

[4] A. Bohr and B. R. Mottelson, Physics of rapidly rotating nuclei, Phys. Today **32**(6), 25 (1979).

[5] R. Clark and B. Wadsworth, *A New Spin on Nuclei* (PhysicsWorld, 1998).

[6] Y. Guo, R. Dubessy, M. G. de Herve, A. Kumar, T. Badr, A. Perrin, L. Longchambon, and H. Perrin, Supersonic Rotation of a Superfluid: A Long-lived Dynamical Ring, Phys. Rev. Lett. **124**, 025301 (2020).

[7] R. K. Kumar, T. Sriraman, H. Fabrelli, P. Muruganandam, and A. Gammal, Three-dimensional vortex structures in a rotating dipolar Bose-Einstein condensate, J. Physics B: At., Mol. Opt. Phys. **49**, 155301 (2016).

[8] R. A. Barankov, Boundary of two mixed bose-einstein condensates, Phys. Rev. A **66**, 013612 (2002).

[9] R. M. Wilson, C. Ticknor, J. L. Bohn, and E. Timmermans, Roton immiscibility in a two-component dipolar Bose Gas, Phys. Rev. A **86**, 033606 (2012).

[10] L. Wen, W. M. Liu, Y. Cai, J. M. Zhang, and J. Hu, Controlling phase separation of a two-component Bose-Einstein condensate, Phys. Rev. A **85**, 043602 (2012).

[11] R. W. Pattinson, T. P. Billam, S. A. Gardiner, D. J. McCarron, H. W. Cho, S. L. Cornish, N. G. Parker, and N. P. Proukakis, Equilibrium solutions for immiscible two-species Bose-Einstein condensates in perturbed harmonic traps, Phys. Rev. A **87**, 013625 (2013).

[12] G. Filatrella, B. A. Malomed, and M. Salerno, Domain walls and bubble droplets in immiscible binary Bose gases, Phys. Rev. A **90**, 043629 (2014).

[13] R. K. Kumar, P. Muruganandam, L. Tomio, and A. Gammal, Miscibility in coupled dipolar and non-dipolar Bose-Einstein condensates, J. Phys. Commun. **1**, 035012 (2017).

[14] R. K. Kumar, L. Tomio, and A. Gammal, Spatial separation of rotating binary Bose-Einstein condensates by tuning the dipolar interactions, Phys. Rev. A **99**, 043606 (2019).

[15] A. L. Fetter, Rotating vortex lattice in a Bose-Einstein condensate trapped in combined quadratic and quartic radial potentials, Phys. Rev. A **64**, 063608 (2001).

[16] E. Lundh, Multiply quantized vortices in trapped Bose-Einstein condensates, Phys. Rev. A **65**, 043604 (2002).

[17] G. M. Kavoulakis and G. Baym, Rapidly rotating Bose-Einstein condensates in anharmonic potentials, New J. Phys. **5**, 51 (2003).

[18] A. L. Fetter, B. Jackson, and S. Stringari, Rapid rotation of a Bose-Einstein condensate in a harmonic plus quartic trap, Phys. Rev. A **71**, 013605 (2005).

[19] A. L. Fetter, Rotating trapped Bose-Einstein condensates, Rev. Mod. Phys. **81**, 647 (2009).

[20] A. Recati, F. Zambelli, and S. Stringari, Overcritical Rotation of a Trapped Bose-Einstein Condensate, Phys. Rev. Lett. **86**, 377 (2001).

[21] K. Kasamatsu, M. Tsubota, and M. Ueda, Giant hole and circular superflow in a fast rotating Bose-Einstein condensate, Phys. Rev. A **66**, 053606 (2002).

[22] P. Engels, I. Coddington, P. C. Haljan, V. Schweikhard, and E. A. Cornell, Observation of Long-Lived Vortex Aggregates in Rapidly Rotating Bose-Einstein Condensates, Phys. Rev. Lett. **90**, 170405 (2003).

[23] U. R. Fischer and G. Baym, Vortex States of Rapidly Rotating Dilute Bose-Einstein Condensates, Phys. Rev. Lett. **90**, 140402 (2003).

[24] V. Bretin, S. Stock, Y. Seurin, J. Dalibard, Fast Rotation of a Bose-Einstein Condensate, Phys. Rev. Lett. **92**, 050403 (2004).

[25] A. Aftalion and I. Danaila, Giant vortices in combined harmonic and quartic traps, Phys. Rev. A **69**, 033608 (2004).

[26] T. P. Simula, A. A. Penckwitt, and R. J. Ballagh, Giant Vortex Lattice Deformations in Rapidly Rotating Bose-Einstein Condensates, Phys. Rev. Lett. **92**, 060401 (2004).

[27] G. Baym and C. J. Pethick, Vortex core structure and global properties of rapidly rotating Bose-Einstein condensates, Phys. Rev. A **69**, 043619 (2004).

[28] M. Correggi, F. Pinsker, N. Rougerie, and J. Yngvason, Rotating superfluids in anharmonic traps: From vortex lattices to giant vortices, Phys. Rev. A **84**, 053614 (2011).

[29] M. Correggi, F. Pinsker, N. Rougerie, and J. Yngvason, Giant vortex phase transition in rapidly rotating trapped Bose-Einstein condensates, Eur. Phys. J. Spec. Top. **217**, 183 (2013).

[30] S. K. Adhikari, Stable controllable giant vortex in a trapped Bose-Einstein condensate, Laser Phys. Lett. **16**, 085501 (2019).

[31] S. Pandey, H. Mas, G. Drougakis *et al.*, Hypersonic Bose-Einstein condensates in accelerator rings, Nature **570**, 205-209 (2019).

[32] E. Lundh, A. Collin and K.-A. Suominen, Rotational States of Bose Gases With Attractive Interactions in Anharmonic Traps, Phys. Rev. Lett. **92**, 070401 (2004).

[33] L. D. Carr and C. W. Clark, Vortices in Attractive Bose-Einstein Condensates in Two Dimensions, Phys. Rev. Lett. **97**, 010403 (2006).

[34] H. Sakaguchi and B. A. Malomed, Localized matter-waves patterns with attractive interaction in rotating potentials, Phys. Rev. A **78**, 063606 (2008).

[35] J. B. Sudharsan, R. Radha, H. Fabrelli, A. Gammal, and B. A. Malomed, Stable multiple vortices in collisionally inhomogeneous attractive Bose-Einstein condensates, Phys. Rev. A **92**, 053601 (2015).

[36] F. Dalfovo, S. Giorgini, L. P. Pitaevskii and S. Stringari, Theory of Bose-Einstein condensation in trapped gases, Rev. Mod. Phys. **71**, 463 (1999).

[37] A. Aftalion, in *Vortices in Bose-Einstein Condensates*, edited by H. Brezis, Progress in Nonlinear Differential Equations and Their Applications Vol. 67 (Birkhäuser Boston, c/o Springer Science+Business Media, New York, USA, 2006).

[38] C. J. Pethick and H. Smith, *Bose-Einstein Condensation in Dilute Gases* (Cambridge University Press, Cambridge, England, 2008).

[39] L. Pitaevskii and S. Stringari, *Bose-Einstein Condensation and Superfluidity* (Oxford University Press, Oxford, 2016).

[40] S. Inouye, M. R. Andrews, J. Stenger, H.-J. Miesner, D. M. Stamper-Kurn, and W. Ketterle, Observation of Feshbach resonances in a Bose-Einstein condensate, Nature (London) **392**, 151 (1998).

[41] C. Chin, R. Grimm, P. Julienne, and E. Tiesinga, Feshbach resonances in ultracold gases, Rev. Mod. Phys. **82**, 1225 (2010).

[42] M. Brtka, A. Gammal and L. Tomio, Relaxation algorithm to hyperbolic states in Gross-Pitaevskii equation, Phys. Lett. A **359**, 339 (2006).

[43] J. Yang, Newton-conjugate-gradient methods for solitary wave computations, J. Comput. Phys. **228**, 7007 (2009).

[44] M. Cozzini, A. L. Fetter, B. Jackson, and S. Stringari, Oscillations of a Bose-Einstein Condensate Rotating in a Harmonic Plus Quartic Trap, Phys. Rev. Lett. **94**, 100402 (2005).

[45] R. P. Feynman, Application of quantum mechanics to liquid helium, in *Progress in Low Temperature Physics*, edited by C. J. Gorter (North-Holland, Amsterdam, 1955), Vol. 1.

[46] E. W. Weisstein, Cassini Ovals, From MathWorld–A Wolfram Web Resource, https://mathworld.wolfram.com/CassiniOvals.html.

[47] L. Wen, H. Xiong and B. Wu, Hidden vortices in a Bose-Einstein condensate in a rotating double-well potential, Phys. Rev. A **82**, 053627 (2010).